tris(polypyridine) couples. Additional structural and vibrational studies, leading to refinements in metal–ligand and intraligand distances, angles, and force constants, might result in further improvements in the agreement between observed and calculated exchange rates, especially for systems in which there is considerable intraligand reorganization and in which a large nonadiabaticity is implicated.

Acknowledgment. We wish to acknowledge very helpful discussions with Drs. Carol Creutz and Bruce Brunschwig and experimental assistance from P. Mulligan (Queens University, Kingston, Ontario, Canada). This work was performed at Brookhaven National Laboratory under contract with the U.S. Department of Energy and supported by its Office of Basic Energy Sciences. D.H.M. wishes to thank the Natural Sciences and Engineering Research Council of Canada for support in the form of a Postdoctoral Fellowship.

Registry No. $Ni(bpy)_3(ClO_4)_3 \cdot 2CH_3CN \cdot 0.5CH_2Cl_2$, 92127-01-0.

Supplementary Material Available: Thermal parameters for the non-hydrogen atoms (Table S1), atomic coordinates for the hydrogen atoms (Table S2), bond distances and angles for the bipyridine rings, the anions, and the solvent molecules (Table S3), observed and calculated structure factors (Table S4), and hydrogen bonds and other close contacts (Table S5) (28 pages). Ordering information is given on any current masthead page.

Contribution from the Institut für Anorganische Chemie, Universität Bern, CH-3000 Bern 9, Switzerland

Transfer of Electronic Excitation Energy in the Antiferromagnets $RbMnCl_3$, $CsMnCl_3$, $CsMnBr_3$, and Rb_2MnCl_4

URSULA KAMBLI† and HANS U. GÜDEL*

Received December 12, 1983

Transfer of electronic excitation energy was studied in crystals of the antiferromagnetic compounds $RbMnCl_3$, $CsMnCl_3$, $CsMnBr_3$, and Rb_2MnCl_4. Nominally pure as well as Er^{3+}- and Nd^{3+}-doped samples were studied by time-resolved luminescence spectroscopy. Both host and guest emissions were followed as a function of concentration, temperature, and time delay after the excitation pulse. There is multiple evidence for excitation transfer. The corresponding rates were quantitatively determined and rationalized in terms of a kinetic model. The transfer to traps is thermally activated, and the activation energies for the four compounds are 537, 1259, 508, and 38 cm^{-1}, respectively. The activation energies are correlated to spectroscopically determined electronic splittings of the $^4T_1$ state. They can be rationalized in terms of a purely excitonic intrasublattice mechanism for long-range energy transfer. No correlation could be established between the energy-transfer characteristics and the dimensionality of the crystal lattice.

1. Introduction

Excitation energy transfer (ET) is a well-known phenomenon in condensed Mn^{2+} compounds. MnF_2[1] as well as the alkali metal fluoromanganates(II) $KMnF_3$, $RbMnF_3$,[2] and $CsMnF_3$[3] have been studied extensively with this respect. ET is very efficient in these compounds down to 4.2 K. As a consequence, there is hardly any intrinsic emission. Most of the emission observed is from Mn^{2+} traps, i.e. Mn^{2+} ions that are slightly perturbed by adjacent impurities such as Ca^{2+}, Zn^{2+}, and Mg^{2+} [4] or by crystal imperfections. Efficient ET at room temperature was also reported for the quasi-1-D antiferromagnets TMMC,[5] $CsMnBr_3$,[6] and $CsMnCl_3 \cdot 2H_2O$,[7] as well as for the alkali metal chloromanganates(II) $CsMnCl_3$[8], $RbMnCl_3$,[8] $KMnCl_3$,[9] and $NaMnCl_3$.[10] In contrast to the fluoride compounds, however, energy transfer is negligible at 4.2 K and the luminescence in these compounds is essentially intrinsic at low temperatures. In the compounds $CsMnCl_3 \cdot 2H_2O$, $RbMnCl_3$, and $CsMnCl_3$, in which fine structure was resolved on the high-energy side of the luminescence band, no trap emission from perturbed Mn^{2+} sites was detected.[11,8]

Energy transfer in the chloromanganates(II) and $CsMnBr_3$ is strongly temperature dependent and becomes efficient only above 50 K. The two-dimensional (2-D) antiferromagnet Rb_2MnCl_4 represents an intermediate case.[12] At 4.2 K ET is not completely absent, but it is not as effective as in MnF_2.

Electronic d–d transitions within the Mn^{2+} ions are spin and parity forbidden. The most likely mechanism for excitation transfer is therefore an exchange mechanism.[13] Exchange interactions in the ground state are responsible for the magnetic properties. A consequence of the exchange coupling in the ground state is the antiferromagnetic order. Exchange pathways depend on structural parameters like bond distances and bridging geometries. Magnetic properties are therefore strongly related to crystal structures. Accordingly, the linear-chain compounds TMMC, $CsMnBr_3$, and $CsMnCl_3 \cdot 2H_2O$ behave as quasi-1-D antiferromagnets, and the layer-structured Rb_2MnCl_4 behaves as a quasi-2-D antiferromagnet.[14–17]

A similar structural dependence is expected for the exchange

† Present address: Institute of Applied Physics, University of Bern, 3012 Bern, Switzerland.

(1) Wilson, B. A.; Yen, W. M.; Hegarty, J.; Imbusch, G. F. *Phys. Rev. B: Condens. Matter* **1979**, *19*, 4238.
(2) (a) Strauss, E.; Gerhardt, V.; Riederer, H. *J. Lumin.* **1976**, *12/13*, 239. (b) Iverson, M. V.; Sibley, W. A. *Phys. Rev. B: Condens. Matter* **1980**, *21*, 2522 and references therein.
(3) Moncorgé, R.; Jacquier, B.; Madej, C.; Blanchard, M.; Brunel, L. C. *J. Phys. (Orsay, Fr.)* **1982**, *43*, 1267.
(4) Greene, R. L.; Sell, D. D.; Feigelson, R. S.; Imbusch, G. F.; Guggenheim, H. J. *Phys. Rev.* **1968**, *171*, 600.
(5) Yamamoto, H.; McClure, D. S.; Marzzacco, C.; Waldman, M. *Chem. Phys.* **1977**, *22*, 79.
(6) McPherson, G. L.; Francis, A. H. *Phys. Rev. Lett.* **1978**, *41*, 1681.
(7) McPherson, G. L.; Willard, S. C. *Chem. Phys. Lett.* **1981**, *78*, 135.
(8) Kambli, U.; Güdel, H. U. *J. Phys. C* **1984**, *17*, 4041.
(9) McPherson, G. L.; Devaney, K. O.; Willard, S. C.; Francis, A. H. *Chem. Phys. Lett.* **1979**, *68*, 9.
(10) Matyushkin, E. V.; Eremenko, V. V.; Bron, R. Y. *J. Magn. Magn. Mater.* **1980**, *15–18*, 1043.
(11) Jia, W.; Strauss, E.; Yen, W. M. *Phys. Rev. B: Condens. Matter* **1981**, *23*, 6075.
(12) Kambli, U.; Güdel, H. U.; Briat, B. *J. Phys. C* **1984**, *17*, 3113.
(13) Dexter, D. L. *J. Chem. Phys.* **1953**, *21*, 836.
(14) Dingle, R.; Lines, M. E.; Holt, S. L. *Phys. Rev.* **1969**, *187*, 643.
(15) Eibschütz, M.; Sherwood, R. C.; Hsu, F. S. L.; Cox, D. E. *AIP Conf. Proc.* **1972**, *No. 10*, 684.
(16) Kobayashi, H.; Tsujikawa, I.; Friedberg, S. A. *J. Low Temp. Phys.* **1973**, *10*, 621.
(17) Witteveen, H. T. *J. Solid State Chem.* **1974**, *11*, 245.

0020-1669/84/1323-3479$01.50/0

interaction in the excited state and for the energy-transfer characteristics. For the linear-chain compound TMMC it was postulated that energy migrates along the chain only and ET is indeed one-dimensional.[5] The high fluorescence yield of intrinsic emission in TMMC in contrast to MnF_2 was explained by the 1-D migration and the corresponding lower trapping probability. Similar arguments were used for $CsMnCl_3 \cdot 2H_2O$[18] (1-D) and $NaMnCl_3$[10] (2-D). The absence of ET at low temperatures, however, is not limited to low-dimensional compounds but is observed for the alkali metal chloromanganates(II) in general. Little attempt has been made so far to rationalize the different temperature dependences of the ET characteristics in the fluoride compounds on one hand and the chloride compounds and $CsMnBr_3$ on the other.

In this paper we report a systematic study of ET characteristics in Mn^{2+} compounds with crystal structures and magnetic properties of different dimensionalities. A very brief report on the same topic was published by McPherson and co-workers.[9]

There is a great structural variety among the alkali metal chloro- and bromomanganates(II). Some compounds adopt strongly anisotropic crystal structures and exhibit low-dimensional magnetic behavior. The title compounds represent all the three dimensionalities. $CsMnBr_3$ crystallizes in the hexagonal $CsNiCl_3$ structure, space group $P6_3/mmc$.[19] Face-sharing octahedra form linear chains along c, with the Cs^+ ions separating the chains. The intrachain nearest-neighbor distance (3.26 Å) is much smaller than the shortest interchain separation (7.61 Å).

$RbMnCl_3$ and $CsMnCl_3$ crystallize in different hexagonal space groups, $P6_3/mmc$ and $R3m$, respectively.[20,21] They are structurally related to $CsMnBr_3$, but the stacking sequence of the face-sharing octahedra is interrupted by corner sharing between fragments of different chains, thus forming a 3-D array.

Rb_2MnCl_4 is a tetragonal perovskite containing layers of corner-sharing $MnCl_6$ octahedra separated by layers of RbCl.[22] The nearest-neighbor Mn–Mn distances within and between the planes are 5.05 and 8.84 Å, respectively.

Inelastic neutron scattering[23,24] and magnetic susceptibility measurements[15,17] show both $CsMnBr_3$ and Rb_2MnCl_4 to be low-dimensional antiferromagnets. The magnon energies exhibit dispersion only along the chain axis ($CsMnBr_3$) or within the plane (Rb_2MnCl_4). The magnetic susceptibility curves have characteristic broad maxima around 85 and 100 K, respectively. Transitions to long-range antiferromagnetic order occur at 8.3 K for $CsMnBr_3$[15] and 56 K for Rb_2MnCl_4.[24]

$CsMnCl_3$ and $RbMnCl_3$ are 3-D Heisenberg antiferromagnets with Neel temperatures of 67[25] and 94 K.[26] They have complicated antiferromagnetic structures.

In order to monitor not only the intrinsic manganese or host emission but also the trap emission, the trivalent lanthanides

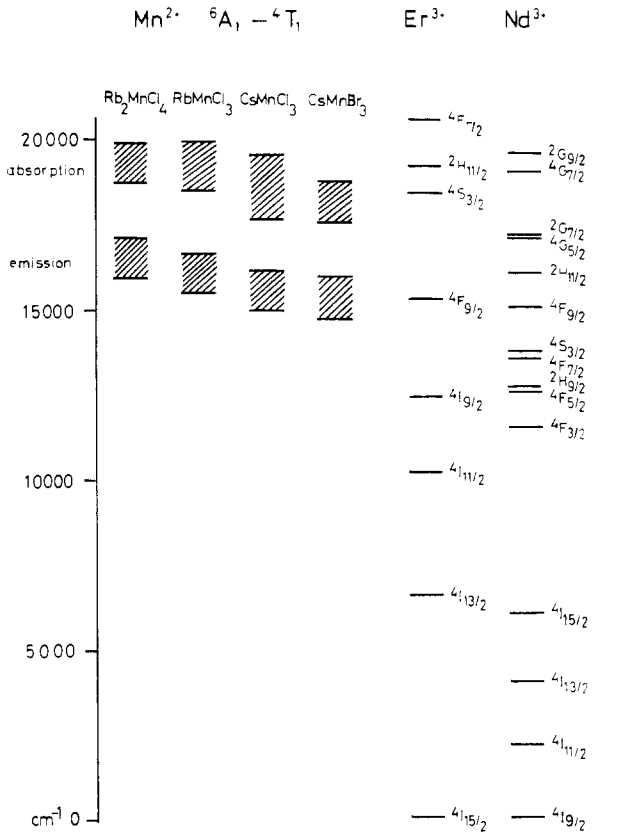

Figure 1. Relevant energy levels of Mn^{2+}, Er^{3+}, and Nd^{3+}.

Er^{3+} and Nd^{3+} were added as radiative probes. Both of these ions have absorption bands in resonance with the manganese emission as shown in Figure 1. They can thus trap the excitation.

2. Experimental Section

The crystals were grown from the melt by the vertical Bridgman method using stoichiometric powders. The preparation of Rb_2MnCl_4, $RbMnCl_3$, and $CsMnCl_3$ was described before.[12,8] For $CsMnBr_3$ the hydrated salt was first prepared by dissolving $MnCO_3 \cdot xH_2O$ (Merck p.A.) in 10% HBr and then adding CsBr (Merck, Suprapur) to the solution in a molar ratio Mn:Cs of 5:1. After slow evaporation of part of the solvent at 50 °C, the crystals were collected, finely ground, and dehydrated by slowly heating them to 300 °C under high vacuum.

For the doped crystals 1 and 0.1 mol % $ErCl_3$, $NdCl_3$, or $ErBr_3$ (Roc/Ric 99.9%) was added to the powders. Care was taken to use starting materials of high purity to minimize the amount of unintentional traps. Oxidized Mn^{3+} and Mn^{4+} traps, however, can be formed by hydrolysis, independent of the quality of the starting materials.[8,12] McPherson and co-workers markedly reduced the content of these oxidized manganese traps by adding a small amount of elemental manganese to the melt.[27]

The samples were checked by powder X-ray diffraction. The lanthanide concentrations were determined by atomic absorption. As the Bridgman technique is a zone refining method, there is a concentration gradient along the boule with the highest concentration on top.

The spectroscopic methods were the same as reported previously.[8,12]

3. Spectroscopic Results

Emission spectra were measured of undoped crystals as well as crystals doped with two different concentrations of Er^{3+} and Nd^{3+}. The Mn^{2+} ions were excited selectively with the 514.5-nm line of an argon laser for $RbMnCl_3$, $CsMnCl_3$, and Rb_2MnCl_4 and with the 568.2-nm line of a krypton laser for $CsMnBr_3$. Er^{3+} and Nd^{3+} have no major absorption bands at these energies, so that direct excitation is negligible. The

(18) Bron, R. Y.; Eremenko, V. V.; Matyushkin, E. V. *Sov. J. Low. Temp. Phys. (Engl. Transl.)* **1979**, *5*, 314.
(19) Goodyear, J.; Kennedy, D. J. *Acta Crystallogr., Sect. B: Struct. Crystallogr. Cryst. Chem.* **1972**, *B28*, 1640.
(20) Goodyear, J.; Steigmann, G. A.; Ali, E. M. *Acta Crystallogr., Sect. B: Struct. Crystallogr. Cryst. Chem.* **1977**, *B33*, 256.
(21) Goodyear, J.; Kennedy, D. J. *Acta Crystallogr., Sect. B: Struct. Crystallogr. Cryst. Chem.* **1973**, *B29*, 744.
(22) Goodyear, J.; Ali, E. M.; Steigmann, G. A. *Acta Crystallogr., Sect. B: Struct. Crystallogr. Cryst. Chem.* **1977**, *B33*, 2932.
(23) Breitling, W.; Lehmann, W.; Weber, R.; Lehner, N. *J. Magn. Magn. Mat.* **1977**, *6*, 113.
(24) Schröder, B.; Wagner, V.; Lehner, N.; Kesharwani, K. M.; Geick, R. *Phys. Status Solidi B* **1980**, *97*, 501.
(25) Melamud, M.; Makovsky, J.; Shaked, H. *Phys. Rev. B: Condens. Matter* **1971**, *3*, 3873.
(26) Melamud, M.; Makovsky, J.; Shaked, H. *Phys. Rev. B: Condens. Matter* **1971**, *3*, 821.
(27) McPherson, G. L.; Talluto, K.; Auerbach, R. A. *Solid State Commun.* **1982**, *43*, 817.

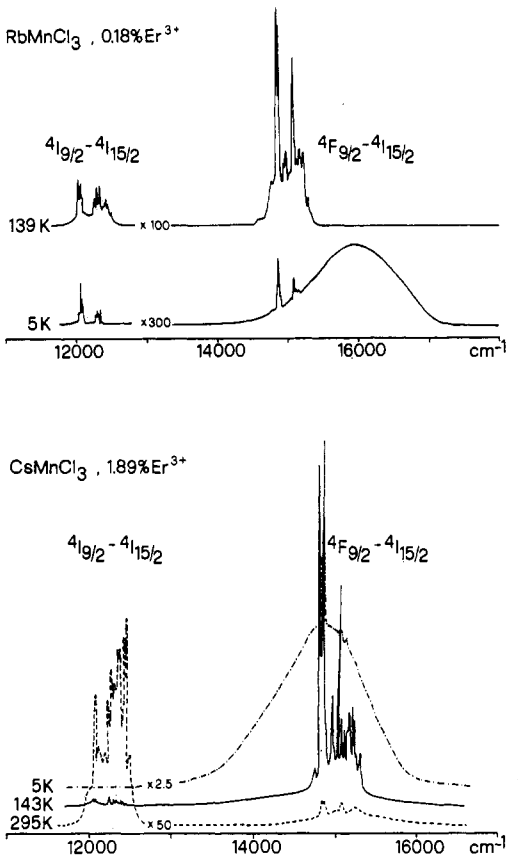

Figure 2. Emission spectra of Er^{3+}-doped $RbMnCl_3$ and $CsMnCl_3$ at selected temperatures. The experimental noise level does not exceed the line thickness.

emission spectra of the doped samples of the four compounds are qualitatively similar. Figure 2 shows, as representative examples, the spectra of $RbMnCl_3$, 0.18% Er^{3+}, and $CsMnCl_3$, 1.89% Er^{3+}, at selected temperatures. Emission is observed from both Mn^{2+} and Er^{3+} ions. They can easily be distinguished. The Mn^{2+} $^4T_1$–$^6A_1$ luminescence appears as a broad featureless band at an energy of approximately 16 000 cm^{-1} for $RbMnCl_3$ and Rb_2MnCl_4 and 15.000 cm^{-1} for $CsMnCl_3$ and $CsMnBr_3$. Er^{3+} exhibits several intense, sharp multiplets. The transitions from $^4F_{9/2}$ and $^4I_{9/2}$ to the $^4I_{15/2}$ ground state are observed around 15 000 and 12 000 cm^{-1}, respectively. The fine structure in the lanthanide emissions is the result of both electronic splittings and vibronic effects and will not be investigated in the present study. The broad-band Mn^{2+} emissions are identical in the doped and undoped samples.

The relative intensities of the Mn^{2+} and Er^{3+} emissions are strongly temperature dependent. All four compounds show qualitatively the same temperature dependence. Representative examples, which also illustrate the concentration dependence of the phenomena, are given in Figure 3.

In the linear-chain host lattice $CsMnBr_3$ and in $CsMnCl_3$, which contains trimeric chain fragments, the Er^{3+} emissions of the strongly doped and the weakly doped samples are practically identical and very similar in the two host lattices. In the linear-chain lattices trivalent impurity ions are likely to cluster in pairs with a vacancy in between for charge compensation.[28]

So, in $CsMnBr_3$ and $CsMnCl_3$ the lanthanide ions appear to be incorporated in a well-defined manner. In $RbMnCl_3$ and Rb_2MnCl_4, on the other hand, the fine structure of the Er^{3+} emission is concentration dependent, indicating multiple sites.

(28) McPherson, G. L.; Varga, J. A.; Nodine, M. H. *Inorg. Chem.* **1979**, *18*, 2189.

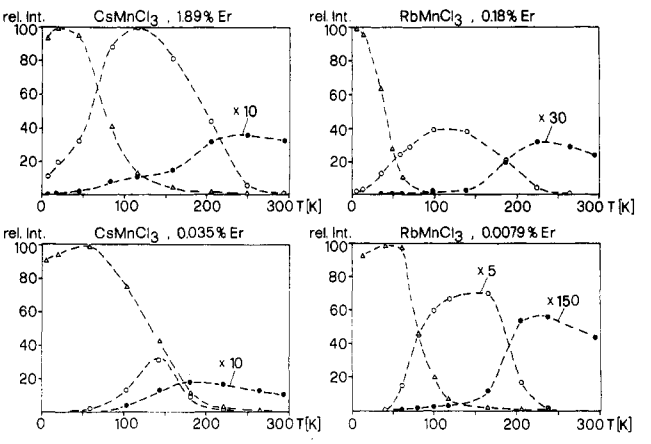

Figure 3. Temperature dependence of the integrated emission intensities of Mn^{2+} and Er^{3+} in $CsMnCl_3$ and $RbMnCl_3$: Δ, Mn^{2+}; ○, Er^{3+} $^4F_{9/2}$; ●, Er^{3+} $^4I_{9/2}$. The broken lines are guides for the eye.

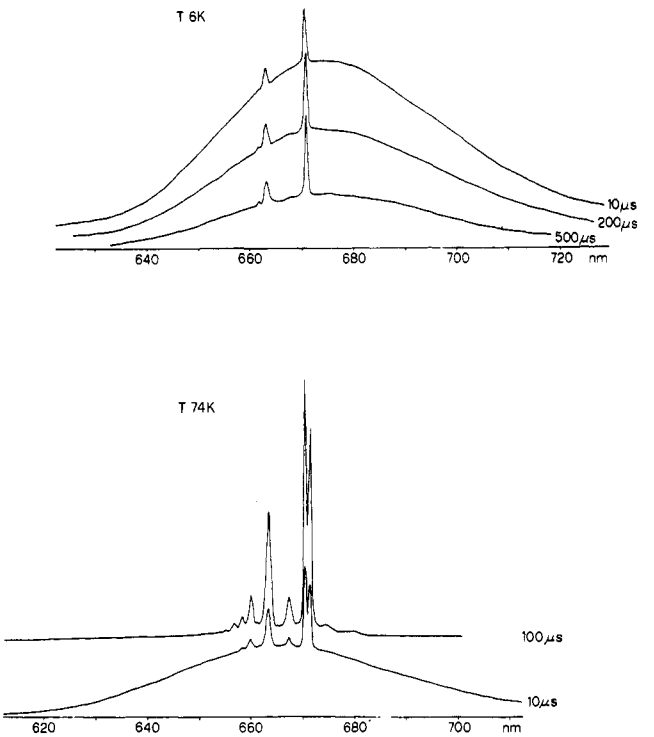

Figure 4. Time-resolved emission spectra of $CsMnBr_3$, 1.78% Er^{3+}, at 6 and 74 K.

Time-resolved emission spectra were measured of all the Er^{3+}-doped lattices. As an example, two sets of spectra of $CsMnBr_3$, 1.78% Er^{3+}, are shown in Figure 4. The Mn^{2+} emission is dominant immediately after the pulse and then decays. Concurrent with this decay is a rise of the Er^{3+} emission intensity. The phenomenon is more pronounced at 74 K than at 6 K, and it is a very nice illustration of the feeding mechanism of the Er^{3+} emission by ET from the Mn^{2+} system.

Similar information is obtained when the emission intensities at a given wavelength are followed as a function of time after the exciting laser pulse. Rise and decay curves of the Mn^{2+} and Er^{3+} $^4F_{9/2}$ emission in the different host lattices are presented in Figure 5. The decay of the Mn^{2+} emission and the rise of the Er^{3+} emission are correlated. They are both governed by the Mn → Er ET rate. The Er^{3+} $^4F_{9/2}$ emission always overlaps with the Mn^{2+} emission. It can therefore not be measured separately, and for a quantitative analysis of the data the Mn^{2+} decay curves will be better suited than the Er^{3+} rise curves. In all the studied compounds of composition $AMnX_3$, the Er^{3+} emission is too weak below 50 K to obtain

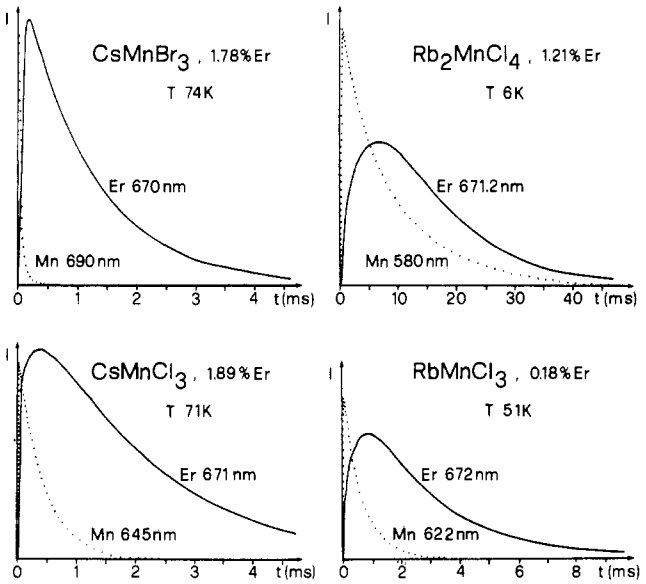

Figure 5. Time dependence after pulsed excitation of the manganese and erbium $^4F_{9/2}$ emission in the different host lattices at selected temperatures.

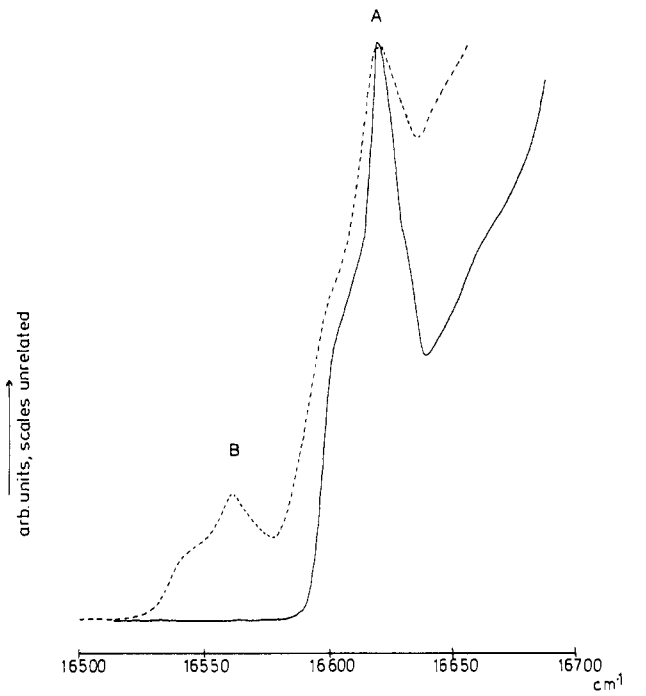

Figure 6. 6 K excitation spectra of the electronic origins of the Mn^{2+} $^6A_1$–$^4T_1$ transition in $CsMnCl_3$, 1.89% Er^{3+}: solid line, the Mn^{2+} emission monitored at 720 nm; dotted line, the Er^{3+} $^4I_{9/2}$ emission monitored at 827.12 nm.

meaningful rise and decay times. For Rb_2MnCl_4, on the other hand, the Er^{3+} luminescence rise is seen already at 6 K (Figure 5).

In the undoped and weakly doped samples of the hexagonal $AMnX_3$ compounds the decay curves of the Mn^{2+} emission are exponential within experimental accuracy. This is no longer the case in crystals with more than 1% Er^{3+}. In these crystals there is a considerable amount of slightly perturbed Mn^{2+} sites in the neighborhood of Er^{3+} ions. These perturbed Mn^{2+} ions can be seen in the low-temperature excitation spectra of the Er^{3+} emission. Figure 6 shows the excitation spectrum of the Er^{3+} as well as the Mn^{2+} emission of $CsMnCl_3$, 1.89% Er^{3+}, in the region of the Mn^{2+} $^6A_1 \leftrightarrow {}^4T_1$ electronic origins. There are two bands (A, B) in the excitation spectrum of the Er^{3+} emission, but only one band (A) in the excitation

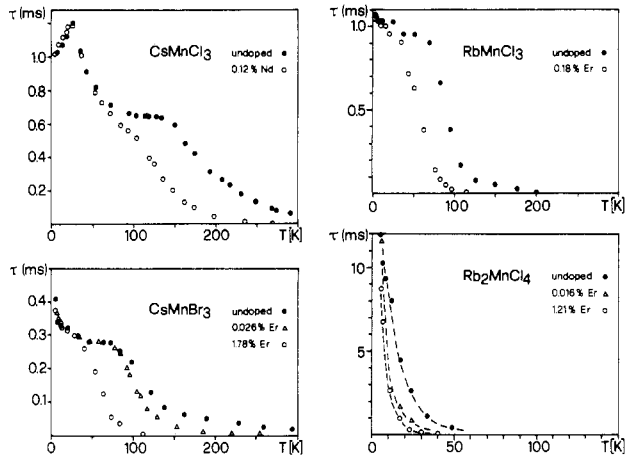

Figure 7. Temperature dependence of the Mn^{2+} emission decay times.

spectrum of the Mn^{2+} emission. The A band is an intrinsic but inhomogeneously broadened feature of the Mn^{2+} system. This is seen from a comparison with the spectra of the undoped crystals.[8] The B band, 60 cm^{-1} to lower energy, belongs to slightly perturbed Mn^{2+} ions in the neighborhood of the Er^{3+} centers. Their high intensity in the Er^{3+} excitation spectrum indicates that the Er^{3+} emission at 6 K is mainly fed from slightly perturbed neighboring Mn^{2+} sites.

In Rb_2MnCl_4 the Mn^{2+} emission is partly intrinsic and partly due to a Mn^{2+} trap with a different decay time and a trap depth of about 250 cm^{-1}.[12] The decay curves are therefore a sum of two exponentials, and they are wavelength dependent. In order to get the decay curves of the intrinsic Mn^{2+} alone they have to be measured on the high-energy tail of the emission band.

The decay times (τ) of the Mn^{2+} emission can be extracted from the decay curves. The quasi-exponential part at longer times was used whenever there were deviations from single exponentials in the strongly doped samples. The decay times are strongly temperature dependent. Doped and undoped samples have qualitatively similar behavior, but the decay times are shorter in the doped samples, indicating an additional decay channel for the Mn^{2+} system in the presence of lanthanide traps. Representative data are shown in Figure 7.

The decay times of the Er^{3+} $^4F_{9/2}$ emission were determined for all host lattices from the decay curves, which are exponential at long times after the pulse. The Er^{3+} decay times are constant below 150 K, and then they decrease exponentially with increasing temperature. $RbMnCl_3$ and $CsMnCl_3$ data are shown as examples in Figure 8.

4. Models for Energy Transfer

4.1. Kinetics. Our situation of host-sensitized ET and luminescence has been discussed in the literature.[29] We adopt the simplest possible model to describe the kinetics of the relevant processes.[30] Excited Mn^{2+} donors may either decay radiatively or decay by ET to traps. Multiphonon relaxation to the ground state can be neglected in the present case, as the energy separation between the $^4T_1$ and $^6A_1$ states of 16000 cm^{-1} is large compared with the highest energy vibrations of about 250 cm^{-1}. Thermal back-transfer from the traps is negligible in the temperature region where k_BT is much smaller than the trap depth. Traps may either be host (H) or lanthanide acceptor (A) traps, both of which decay radiatively, or quenching traps (Q). Unintentional impurities of transition-metal ions like Mn^{3+}, Fe^{2+}, Co^{2+}, Ni^{2+} and Cu^{2+} are the most likely quenching traps. The energy levels and rate parameters of the different decay processes are represented in

(29) Powell, R. C.; Blasse, G. *Struct. Bonding (Berlin)* **1980**, *42*, 43.
(30) Powell, R. C.; Soos, Z. G. *Phys. Rev. B: Condens. Matter* **1972**, *5*, 1547.

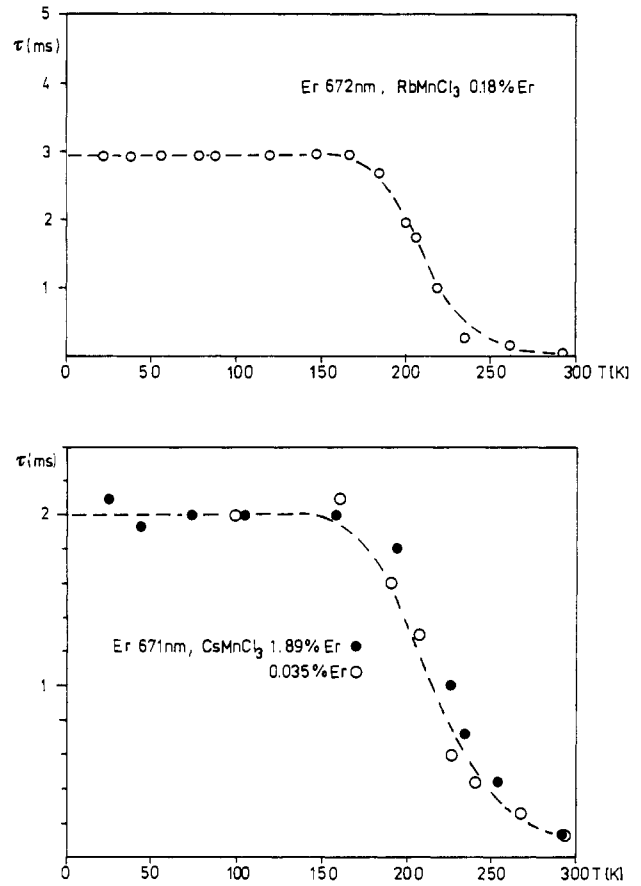

Figure 8. Temperature dependence of the Er^{3+} $^4F_{9/2}$ emission decay times in $RbMnCl_3$ and $CsMnCl_3$. The dotted lines are calculated according to eq 11 with the parameters of Table III.

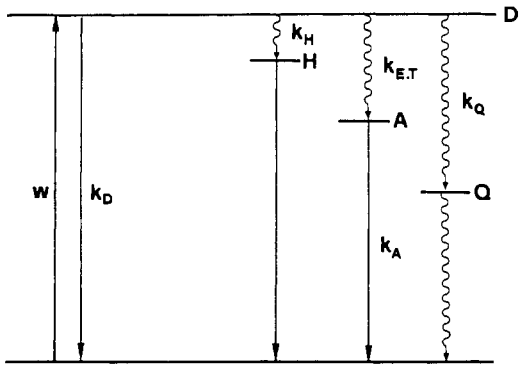

Figure 9. Schematic representation of the energy levels and rate parameters for energy transfer in the presence of different kinds of traps.

Figure 9. The time dependence of the donor (D) and acceptor (A) luminescence in this model is given by

$$dN_D/dt = w - k_D N_D - k_H N_D - k_{ET} N_D - k_Q N_D \quad (1)$$

$$dN_A/dt = k_{ET} N_D - k_A N_A \quad (2)$$

where w represents the excitation rate of the host, k_D and k_A are the radiative decay rates, and k_H, k_{ET}, and k_Q are the transfer rates to host traps, acceptors, and quenchers, respectively. The solutions to eq 1 and 2 for δ-pulse excitation and initial conditions $N_D(0) = 1$, $N_A(0) = 0$ are[30]

$$N_D(t) = e^{-(k_D+k_H+k_{ET}+k_Q)t} \quad (3)$$

$$N_A(t) = [k_{ET}/(k_A - k_D - k_H - k_{ET} - k_Q)] \times (e^{-(k_D+k_H+k_{ET}+k_Q)t} - e^{-k_A t}) \quad (4)$$

The donors decay exponentially, with a rate corresponding to the sum of the rates of all depleting processes. The time dependence of the acceptor emission is characterized by an initial rise due to the feeding term given by the decay of donors and after depletion of the donors by an exponential decay characteristic for the acceptor.

Donor and acceptor decay curves yield the same information about energy-transfer rates. In the specific compounds studied in this paper the Er^{3+} $^4F_{9/2}$ emission is superimposed on the Mn^{2+} emission, whereas the Mn^{2+} decay can be measured separately and will be used for the analysis. k_{ET}, as defined in this simple model, represents the nonradiative ET to the lanthanide centers. It is therefore zero in the undoped systems, and it can be determined from the difference of the donor decay rates of the doped and undoped crystals at a given temperature, with the assumption of k_H and k_Q being equal in the two crystals:

$$k_{ET} = k_{doped} - k_{undoped} = 1/\tau_{doped} - 1/\tau_{undoped} \quad (5)$$

Mechanistically, this transfer rate includes migration of excitation within the Mn^{2+} host as well as the trapping process at the lanthanide site. Two limiting cases are important and make it possible to separate exciton diffusion and trapping.

Trapping Limited Case. Excitation diffusion within the host lattice is much faster than the single-step transfer at the trapping site. The rate for nearest-neighbor donor–acceptor transfer is given by[31]

$$k_{ET} = x_A \sum_{nn} k_{DA} \quad (6)$$

where x_A is the molar fraction of acceptors, k_{DA} is the single-step donor–acceptor transfer rate, and the sum includes all the nearest-neighbor donors of a given acceptor. In this case no information is obtained about migration within the host.

Diffusion Limited Case. If the transfer rate between host sites is smaller than the trapping rate, the diffusion within the host lattice is the rate-determining process. The energy diffusion can be described by a random-walk model. For 3-D isotropic diffusion the rate becomes[32,33]

$$k_{ET} = x_A P k_{DD} \quad (7)$$

where P is a lattice dependent constant (about 0.7 for cubic lattices) and k_{DD} is the single-step transfer rate between donors. As in the process (6), the transfer rate depends linearly on the acceptor concentration.

In the case of low-dimensional diffusion, a different concentration dependence of the transfer rate is obtained with the random-walk model.[32,34] A quadratic concentration dependence is obtained for 1-D diffusion and a logarithmic dependence for 2-D diffusion in a quadratic lattice:[32,34]

$$\text{1-D:} \quad k_{ET} = x_A^2 k_{DD} \quad (8)$$

$$\text{2-D:} \quad k_{ET} = k_{DD} x_A/(1 - \ln x_A) \quad \text{for } x_A < 10^{-3} \quad (9)$$

The decay curves of the donor emission become nonexponential in the limit of low-dimensional diffusion. Different expressions for the donor decay in presence of 1-D and 2-D diffusion were derived by Huber[31,35] and Wieting and coworkers.[36] It was pointed out in ref 36, however, that already very small deviations from strictly 1-D behavior yield exponential decay curves. Due to this as well as the limited experimental accuracy it will be difficult to discriminate between

(31) Huber, D. L. *Phys. Rev. B: Condens. Matter* **1979**, *20*, 2307.
(32) Oelkrug, D.; Wölpl, W.; Kempny, W.; Kayser, W. *Ber. Bunsenges. Phys. Chem.* **1976**, *80*, 441.
(33) Montroll, E. W.; Weiss, G. H. *J. Math. Phys. (N. Y.)* **1956**, *6*, 167.
(34) Montroll, E. W. *Proc. Int. Conf. Stat. Mech.* **1969**, *26*, 6.
(35) Ghosh, K. K.; Huber, D. L. *J. Lumin.* **1980**, *21*, 225.
(36) Wieting, R. D.; Fayer, M. D.; Dlott, D. D. *J. Chem. Phys.* **1978**, *69*, 1996.

Table I. Activation Energies (Δ) and Rates $(k_{ET})_{T\to\infty}$ for Energy Transfer to the Lanthanide Traps (Donor-Donor Transfer Rates (k_{DD}) Calculated According to Eq 7)

	$RbMnCl_3$				$CsMnCl_3$			
A	x_A	$(k_{ET})_{T\to\infty}$, s^{-1}	$(k_{DD})_{T\to\infty}$, s^{-1}	Δ, cm^{-1}	x_A	$(k_{ET})_{T\to\infty}$, s^{-1}	$(k_{DD})_{T\to\infty}$, s^{-1}	Δ, cm^{-1}
Er^{3+}	1.8×10^{-3}	5.7×10^{7}	4.5×10^{10}	529	1.9×10^{-2}			
	7.9×10^{-5}	2.7×10^{6}	4.8×10^{10}	530	3.5×10^{-4}	2.7×10^{8}	1.8×10^{12}	1268
Nd^{3+}	9.4×10^{-4}	2.7×10^{7}	4.1×10^{10}	552	1.2×10^{-3}	1.8×10^{8}	2.1×10^{11}	1255
	$CsMnBr_3$				Rb_2MnCl_4			
A	x_A	$(k_{ET})_{T\to\infty}$, s^{-1}	$(k_{DD})_{T\to\infty}$, s^{-1}	Δ, cm^{-1}	x_A	$(k_{ET})_{T\to\infty}$, s^{-1}	$(k_{DD})_{T\to\infty}$, s^{-1}	Δ, cm^{-1}
Er^{3+}	1.8×10^{-2}	1.8×10^{8}	1.4×10^{10}	507	1.2×10^{-2}	3.6×10^{5}	4.3×10^{7}	38
	2.6×10^{-4}	9.3×10^{6}	1.8×10^{10}	508	1.6×10^{-4}	6.0×10^{3}	5.4×10^{7}	

the different models. In addition, deviations from exponential decay curves can also have other causes such as the presence of more than one emitting center.

4.2. Temperature Dependence of Transfer Rates. In our Mn^{2+} compounds the following three physical effects may contribute to temperature dependent rates:

(1) In antiferromagnetically ordered materials, excitonic ET between nearest neighbors on opposite sublattices is spin forbidden, as it requires a change of spin projection $\Delta M_s = 2$.[37] The change in spin projection can be compensated for by two magnons, i.e. intersublattice transfer can occur with a magnon-assisted process.[37] This is a thermally activated process depending on the magnon population. We thus have a rather intriguing situation: On the one hand, ET can occur as a consequence of exchange coupling between nearest neighbors, one of which is electronically excited. On the other hand, ground-state exchange interactions lead to antiferromagnetic order, which sets a barrier to nearest-neighbor transfer.

(2) Lattice relaxation in the excited state is another reason for exciton localization or "self-trapping". If there is a marked difference between the equilibrium geometries of ground and excited states, relaxation may take place before transfer can occur.[13] Resonant $Mn^{2+} \to Mn^{2+}$ transfer is then inhibited, and the potential barrier due to this self-trapping has to be overcome by thermal activation.[30] This restriction does not hold for $Mn^{2+} \to Er^{3+}$, Nd^{3+} nearest-neighbor transfer. As is seen from Figure 1, Er^{3+} and Nd^{3+} have absorption bands in resonance with the Mn^{2+} emission. We therefore expect nearest-neighbor $Mn^{2+} \to Er^{3+}$, Nd^{3+} transfer to be efficient down to the lowest temperatures.

(3) Purely excitonic transfer is formally allowed only within sublattices. It is governed by excitation-transfer integrals between next-nearest neighbors on the same sublattice, which are expected to be small and dependent on the nature of the exciton involved. Thermal population of more than one excitonic state can thus lead to a temperature dependence of intrasublattice ET. In MnF_2, e.g., it was found that ET was more efficient through the exciton channel E2, lying 10–20 cm^{-1} above E1.[1]

5. Discussion

5.1. $Mn^{2+} \to Er^{3+}$, Nd^{3+} Excitation Transfer. From the spectroscopic data there is multiple evidence for efficient ET from the manganese host to the lanthanide traps in all the compounds above 50 K. Emission of Er^{3+} and Nd^{3+} is observed on selective excitation of the Mn^{2+} ions. The Er^{3+} $^4F_{9/2}$ emission dominates the spectrum in all the samples at 140 K. Its intensity is orders of magnitude too high for direct excitation of ions with very small absorption coefficients in low concentration. The Er^{3+} luminescence rise observed in the time-resolved spectra is characteristic for trap emission being fed via ET.

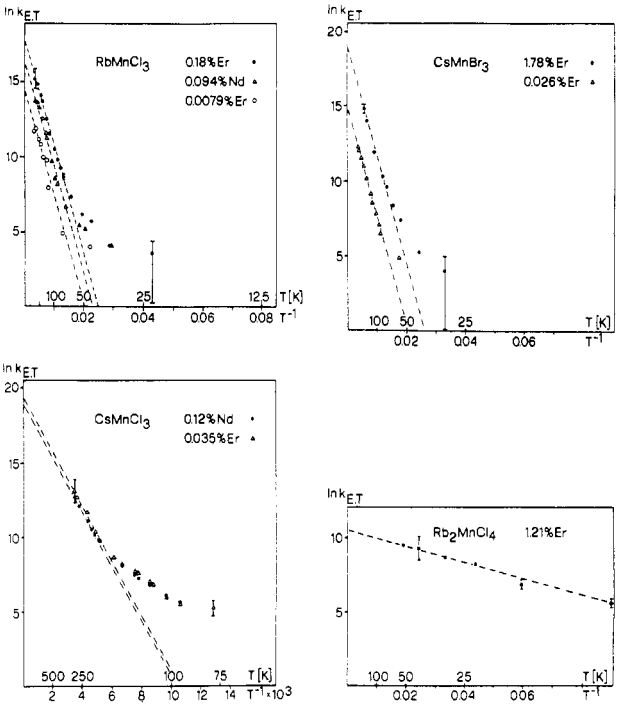

Figure 10. Temperature dependence of the rates for energy transfer to the lanthanides.

The temperature dependence of relative intensities of Mn^{2+} and Er^{3+} emission (Figure 3) and of the decay times of the Mn^{2+} emission (Figure 7) indicates that the overall ET to traps is a thermally activated process. The overall transfer rates to the lanthanides (k_{ET}) and the thermal activation energies for this transfer can be determined from the intensity data as well as from the lifetime data. The first method can lead to incorrect results when Mn^{2+} traps (host traps) contribute to the emission. This is the case in Rb_2MnCl_4.[12] As the intrinsic and trap emissions are not spectrally resolved, the intensity data yield only the sum of both emissions, but it is important to measure the intrinsic emission separately. This is possible by using the decay curves at the high-energy tail of the emission band. The overall transfer rates to the lanthanides (k_{ET}) were determined from the lifetime data of the doped and undoped crystals using eq 5. The advantage of this procedure is that the lanthanide concentrations are known and all the terms of the unknown impurities cancel out.

The transfer rates are very small at 5 K ($<10^2$ s^{-1}) for all the compounds. They increase exponentially with increasing temperature, and the temperature dependence can be described with the empirical activation law

$$k_{ET}(T) = (k_{ET})_{T\to\infty} e^{-\Delta/k_B T} \qquad (10)$$

where Δ is the activation energy for the transfer process. Plots of ln k_{ET} vs. T^{-1} are shown for all host lattices in Figure 10. All the curves show a linear dependence on T^{-1} at high tem-

(37) Ueda, K.; Tanable, Y. *J. Phys. Soc. Jpn.* **1980**, *48*, 1137.

peratures. From the linear part of the curves the activation energies and the transfer rates for $T \rightarrow \infty$ can be determined. The values obtained are summarized in Table I.

The activation energies for ET are markedly different in the four compounds. They are several hundred wavenumbers in the hexagonal $AMnX_3$ compounds and only 38 cm^{-1} in Rb_2MnCl_4. The activation energies are independent of the nature of traps. We therefore conclude that they are characteristic for the transfer within the manganese host and not for the trapping at the lanthanide site. At 5 K the migration within the manganese host is negligibly small in the $AMnX_3$ lattices. The residual Er^{3+} emission intensity at 5 K arises from direct transfer to Er^{3+} traps from neighboring Mn^{2+} ions. This follows from the appearance of the bands of perturbed near-neighbor Mn^{2+} ions in the excitation spectrum of Er^{3+} (Figure 6). The rise of the Er^{3+} $^4F_{9/2}$ emission in $CsMnCl_3$ is relatively fast at 6 K (<100 μs) due to this single-step $Mn^{2+} \rightarrow Er^{3+}$ transfer. Around 70 K, in the temperature region where exciton migration within the manganese system is becoming effective, there is a slower rise (~500 μs) characteristic for $Mn \rightarrow Mn$ transfer.

5.2. Energy Migration and Dimensionality. As the energy diffusion within the Mn^{2+} system is thermally activated there is a temperature region where the transfer is diffusion limited. In the case of low-dimensional diffusion the decay curves of the host emission are expected to be nonexponential (section 4.1). The experimental decay curves of the Mn^{2+} emission in $CsMnBr_3$, however, are exponential at all temperatures in the pure and weakly doped samples. The same is true for the intrinsic emission in Rb_2MnCl_4. In crystals containing 1–2% Er^{3+}, on the other hand, nonexponential behavior was observed in all the hexagonal compounds between 50 and 100 K and in Rb_2MnCl_4 below 40 K. There is a considerable concentration of perturbed Mn^{2+} sites (5–10%) in these crytals, and multiple-site luminescence is the consequence. In the temperature region where these trap sites are being fed by ET and back-transfer is not yet thermally accessible, the decay curves are a sum of exponentials.

None of the observed deviations from exponential behavior could thus be attributed to anisotropic diffusion. Furthermore, a comparison of the transfer rates of $CsMnBr_3$ doped with two different concentrations of Er^{3+} showed a linear concentration dependence, as expected for 3-D diffusion. Yamamoto and co-workers,[5] on the other hand, found a quadratic dependence on trap concentration for the transfer rate in TMMC doped with Co^{2+} and Cu^{2+} as predicted by the 1-D random-walk model (section 4.1).

We conclude that, on the basis of the present data, it is not possible to establish anisotropic diffusion in $CsMnBr_3$ and Rb_2MnCl_4. The qualitative and quantitative behavior of $CsMnBr_3$ is very similar to that of the other hexagonal compounds $RbMnCl_3$ and $CsMnCl_3$.

It is possible that the 1-D and 2-D character of $CsMnBr_3$ and Rb_2MnCl_4, respectively, is not pronounced enough to produce the deviations from exponential behavior, as predicted by the theoretical models. The different concentration dependence found for $CsMnBr_3$ and TMMC would point in that direction, since TMMC is one of the best known realizations of a 1-D antiferromagnet. Another possibility is that the deviations from nonexponential behavior are smaller than our experimental accuracy and thus escape measurement.

5.3. Thermal Activation of Excitation Transfer within the Manganese System. The striking feature of Rb_2MnCl_4 is the far lower activation energy for energy migration, an activation energy of the order of magnitude found in manganese fluoride compounds. It appears that the lattices investigated so far can be divided into two groups with either large or small activation energies for ET, depending on whether they behave in a "localized" or "delocalized" manner at low temperatures in terms of exciton motion. The first group consists of $CsMnCl_3$, $RbMnCl_3$, $CsMnBr_3$, $CsMnCl_3 \cdot 2H_2O$, TMMC, and $NaMnCl_3$, with activation energies of the order of several hundred wavenumbers. Members of the second group are MnF_2, $RbMnF_3$, $KMnF_3$, $CsMnF_3$, and Rb_2MnCl_4. For the manganese fluoride compounds activation energies of the order of 10–20 cm^{-1} were reported.[1,2a,3]

Table II. Activation Energies (Δ) for Energy Transfer in Different Mn^{2+} Compounds and (I) Trigonal Splitting and (II) Energetic Splitting between the Two Lowest Levels of the $^4T_1$ State

I	$RbMnCl_3$	$CsMnCl_3$	$CsMnBr_3$
Δ,[a] cm^{-1}	537	1259	508
$E(^4A_2) - E(^4E)$	~200–500[b]	1100[b]	~200–500
II	Rb_2MnCl_4	MnF_2	$KMnF_3$
Δ, cm^{-1}	38	11[d]	7[d]
$E2 - E1$	~10–100[c]	17[d]	12[d]

[a] Mean of values of Table I. [b] Reference 8. [c] Reference 12. [d] Reference 1.

We want to discuss in some detail the questions of why the activation energies are so different in the two groups and which of the mechanisms discussed in section 4.2 are most likely to be operative. TMMC, $CsMnCl_3 \cdot 2H_2O$, and $NaMnCl_3$ have all been discussed in terms of mechanisms 1 and 2, i.e. magnon-assisted transfer and lattice relaxation, respectively.[5,11,10] In the very detailed studies of MnF_2[1] and related compounds,[3] on the other hand, the observed activation energies were attributed to mechanism 3, i.e. purely excitonic intrasublattice transfer through exciton E2, lying 10–20 cm^{-1} above E1. It is not obvious why mechanisms 1 and 2 should be active, thus increasing the activation energy by 1–2 orders of magnitude, in one group of antiferromagnetic Mn^{2+} compounds but not in the other. Our results for the hexagonal $AMnX_3$ lattices will hopefully shed some more light on this question.

Beginning with mechanism 1, zone boundary magnon energies for all the compounds studied here are of the order of 80 cm^{-1}. Magnon-assisted intersublattice transfer is therefore expected to be activated in the temperature range 20–80 K. But, the observed activation energies for ET to traps of 1259, 537, and 508 cm^{-1}, respectively, are far too large to be accounted for by a magnon-assisted mechanism. The situation is different for Rb_2MnCl_4. The activation energy of 38 cm^{-1} could result from this mechanism.

Mechanism 2, i.e. thermal activation as a result of lattice relaxation, has to be discounted as well, because it cannot explain the large difference in activation energy between the two groups. All the compounds have similar band widths and Stokes shifts of the $^6A_1 \leftrightarrow {}^4T_1$ transitions. The difference in potential surfaces between the ground and the excited states and thus the activation energies for ET after thermal relaxation are therefore expected to be similar.

Mechanism 3, i.e. purely excitonic ET within a sublattice, depends on the energy splitting of the $^4T_1$ state. The combined action of an axial crystal field component, spin–orbit coupling, and the exchange field completely removes the degeneracy of $^4T_1$. If the axial crystal field is of the same order or smaller than spin–orbit coupling and exchange field, the total energy spread of the 12 levels is 100–200 cm^{-1}.[12] Such a situation is realized in MnF_2, $RbMnF_3$, $KMnF_3$, and Rb_2MnCl_4. If the axial field is large compared to spin–orbit coupling and exchange field, there is a first-order splitting of $^4T_1$ into the orbital components $^4A_2$ and ^4E. This situation is found in the hexagonal compounds $CsMnCl_3$, $RbMnCl_3$, and $CsMnBr_3$.[8] In Table II the activation energies are compared with the spectroscopically estimated trigonal splittings of $^4T_1$ for the hexagonal compounds. Included in the table are activation energies and E2–E1 exciton splittings for cubic or nearly cubic

Table III. Rates $[(1/\tau_{BT})_{T\to\infty}]$ and Activation Energies (Δ) for Back-Transfer from the Er^{3+} $^4F_{9/2}$ Level and Trap Depth Obtained from Spectroscopic Data

	$RbMnCl_3$	$CsMnCl_3$	$CsMnBr_3$	Rb_2MnCl_4
$(1/\tau_{BT})_{T\to\infty}$, s^{-1}	5.6×10^8	1.6×10^7	7.8×10^8	3.6×10^9
Δ, cm^{-1}	2080	1540	1280	2680
Mn^{2+} ($^4T_1$)-Er^{3+} ($^4F_{9/2}$) trap depth, cm^{-1}	2250[a]	1450[a]	1300	2470[b]

[a] Reference 8. [b] Reference 12.

compounds. There is a striking correlation between activation energies for ET on the one hand and the spectroscopic energy differences. This suggests that, as in MnF_2, energy transfer is far more efficient via a higher lying electronic level also in the hexagonal compounds. In these lattices, the distortion is a trigonal elongation of the MnX_6 cluster[19-21] and the ^4E component has lowest energy.[38] Energy transfer appears to be more efficient via the $^4A_2$ state. Intuitively, this makes sense, because the exchange coupling between neighboring Mn^{2+} ions is dominated by one or two orbital components with favorable overlap. In a study of trigonal $Mn_2Br_9^{5-}$ and $Mn_2Cl_9^{5-}$ pair excitations, the $t_{a_1} \leftrightarrow t_{a_1}$ pathway was found to provide a dominant contribution to the exchange coupling in the ground state and the $^4A_1$ excited state.[39] It can be shown that t_{a_1} orbitals are involved in the $^4A_2$ excitation, and they are therefore likely to provide a dominant contribution to the excitation transfer.

In Rb_2MnCl_4 the tetragonal crystal field component is estimated to be less than 100 cm^{-1}, leading to a splitting pattern similar to that found in MnF_2.[12] The exciton level E2, corresponding to the $^4T_1$ (0, $^3/_2$) component (M_L, M_S notation), has not been spectroscopically localized so far in Rb_2MnCl_4. It is expected to lie between 10 and 100 cm^{-1} above $^4T_1$ (1, $^3/_2$), the E1 exciton,[12] and the experimental activation energy of 38 cm^{-1} could well correspond to that energy difference.

5.4. $Er^{3+} \to Mn^{2+}$ Back-Transfer. The temperature dependence of the Er^{3+} $^4F_{9/2}$ emission intensity passes through a maximum around 150 K in all the host lattices. The intensity increase below 150 K is due to the increasing efficiency of the thermally activated feeding process from the Mn^{2+} system. The intensity decrease above 150 K concurs with a decrease of the decay times (Figure 8). Both of these effects are due to a nonradiative excitation decay of the Er^{3+} centers. This can either be back-transfer to the Mn^{2+} system or multiphonon relaxation to a lower Er^{3+} level. In the case of back-transfer the temperature dependence of the decay time can be described by the empirical activation law

$$1/\tau = 1/\tau_R + (1/\tau_{BT})_{T\to\infty} e^{-\Delta/k_B T} \qquad (11)$$

where τ_R is the radiative lifetime, $(1/\tau_{BT})_{T\to\infty}$ the rate for back-transfer, and Δ the activation energy corresponding to the trap depth. The trap depth can be determined independently from spectroscopic data.

The parameter values obtained by fitting eq 11 to the experimental data are listed in Table III together with the energy difference between the lowest energy exciton of the Mn^{2+} system[8,12] and the center of the Er^{3+} $^4F_{9/2}$ emission. There is an excellent correlation between the two sets of data, suggesting that back-transfer is the dominating depletion mechanism for the $^4F_{9/2}$ level of Er^{3+} above 150 K.

6. Conclusions

Transfer of electronic excitation energy can be shown to occur in the compounds $RbMnCl_3$, $CsMnCl_3$, $CsMnBr_3$, and Rb_2MnCl_4. The transfer process is thermally activated with pronounced differences in activation energy between the various compounds. The dimensionality of the crystal lattice appears to be of minor importance in determining the ET behavior. The hexagonal compounds of composition $AMnX_3$ all have, like TMMC, large activation energies of several hundered wavenumbers, independent of dimensionality. Rb_2MnCl_4, on the other hand, with an activation energy of 38 cm^{-1}, has an ET and luminescence behavior, which somewhat resembles that of MnF_2 and related fluoromanganates(II) with small activation energies.

The different ET characteristics of the two classes of compounds can be rationalized in terms of their dependence on the size of the axial crystal field distortion of the complexes. A purely excitonic transfer mechanism appears to be responsible for the large activation energies found in the hexagonal compounds. In MnF_2 and related compounds this excitonic barrier is overcome at temperatures below 10 K already. The other possible mechanisms for thermal ET activation have some influence on the luminescence and ET behavior at higher temperatures, but they are of minor importance for the long-range ET behavior. In the hexagonal compounds the order of effects is reversed, but again the excitonic mechanism determines the long-range ET characteristics. Short-range ET between neighboring Mn^{2+} ions on different sublattices is made possible by a thermally activated multimagnon process in the temperature range 20–80 K. Long-range ET is still inhibited in this temperature range, because the excitonic intrasublattice transfer is not efficient. Through the population of the $^4A_2(^4T_1)$ trigonal component at higher temperatures, a much more efficient excitation transfer pathway is opened up.

Acknowledgment. We thank N. Furer for preparing some of the crystals. This work was financially supported by the Swiss National Science Foundation.

Registry No. $RbMnCl_3$, 14219-55-7; $CsMnCl_3$, 14219-53-5; $CsMnBr_3$, 36482-50-5; Rb_2MnCl_4, 15629-32-0; Er^{3+}, 18472-30-5; Nd^{3+}, 14913-52-1.

(38) Hempel, J. *J. Chem. Phys.* **1976**, *64*, 4307.
(39) McCarthy, P. J.; Güdel, H. U. *Inorg. Chem.* **1984**, *23*, 880.